Research Paper

Iodinated Echogenic Glycol Chitosan Nanoparticles for X-ray CT/US Dual Imaging of Tumor

Daeil Choi[1,2], Sangmin Jeon[1,3], Dong Gil You[1,3], Wooram Um[1,3], Jeong-Yeon Kim[4], Hong Yeol Yoon[1], Hyeyoun Chang[1], Dong-Eog Kim[4], Jae Hyung Park[3], Hyuncheol Kim[2] and Kwangmeyung Kim[1,5✉]

1. Center for Theragnosis, Biomedical Research Institute, Korea Institute of Science and Technology, 5, Hwarang-ro 14-gil, Seongbuk-gu, Seoul 02792, Republic of Korea
2. Department of Chemical and Biomolecular Engineering and Interdisciplinary Program of Integrated Biotechnology, Sogang University, 35, Baekbeom-ro, Mapo-gu, Seoul 04107, Republic of Korea
3. School of Chemical Engineering, Sungkyunkwan University, 2066, Seobu-ro, Jangan-gu, Suwon 16419, Republic of Korea
4. Molecular Imaging and Neurovascular Research Laboratory, Dongguk University College of Medicine, Goyang 10326, Repulblic of Korea
5. KU-KIST Graduate School of Converging Science and Technology, Korea University, 145 Anam-ro, Seongbuk-gu, Seoul, 02841, Republic of Korea

✉ Corresponding author: Kwangmeyung Kim, Ph.D. Tel: +82-2-958-5916; fax: +82-2-958-5909; e-mail: kim@kist.re.kr

Abstract

Development of biopolymer-based imaging agents which can access rapidly and provide detailed information about the diseases has received much attention as an alternative to conventional imaging agents. However, development of biopolymer-based nanomaterials for tumor imaging still remains challenging due to their low sensitivity and image resolution. To surmount of these limitations, multimodal imaging agents have been developed, and they were widely utilized for theranostic applications. Herein, iodine containing echogenic glycol chitosan nanoparticles are developed for x-ray computed tomography (CT) and ultrasound (US) imaging of tumor diagnosis. X-ray CT/US dual-modal imaging probe was prepared by following below two steps. First, iodine-contained diatrizoic acid (DTA) was chemically conjugated to the glycol chitosan (GC) for the CT imaging. DTA conjugated GC (GC-DTA NPs) formed stable nanoparticles with an average diameter of 315 nm. Second, perfluoropentane (PFP), a US imaging agent, was physically encapsulated into GC-DTA NPs by O/W emulsion method yielding GC-DTA-PFP nanoparticles (GC-DTA-PFP NPs). The GC-DTA-PFP NPs formed nanoparticles in physiological condition, and they presented the strong x-ray CT, and US signals in phantom test in vitro. Importantly, GC-DTA-PFP NPs were effectively accumulated on the tumor site by enhanced permeation and retention (EPR) effects. Moreover, GC-DTA-PFP NPs showed x-ray CT, and US signals in tumor tissues after intratumoral and intravenous injection, respectively. Therefore, GC-DTA-PFP NPs indicated that x-ray CT/US dual-modal imaging using iodinated echogenic nanoparticles could be provided more comprehensive and accurate diagnostic information to diagnosis of tumor.

Key words: Glycol chitosan nanoparticles, Computed tomography, Ultrasound imaging, Tumor imaging, Dual-modal imaging

Introduction

Over the past decade, multi-modal imaging have utilized for cancer treatment since they can provide early diagnosis, determination of the stage, assistance of therapeutic regimens, and monitoring the efficacy of therapeutics. Recently, various types of nanoparticle have developed for multimodal imaging, which combination of two or more contrasts for the more accurate and timely imaging of desired lesions.[1, 2] In addition, combination with conventional diagnosis approaches such as computed tomography (CT), magnetic resonance imaging (MRI), positron emission tomography (PET), optical imaging and ultrasound (US) imaging, multi-modal imaging agents can provide anatomical and physiological

changes of cancer.[3, 4] However, despite various multi-modal imaging agents were developed for combination of several diagnosis approaches, organization of appropriate imaging approaches and designation of multi-modal imaging agents remain challenging. In this point of view, Xu et al., have proposed marriage design concept of structure and composition by using Au nanocrystal/hollow mesoporous silica nanoparticle/Au nanoparticle/ manganese oxide-based tri-modal imaging contrast agent, which could be utilized for US, MR and CT imaging.[5]

Among the diagnosis approaches, Ultrasound (US) imaging is widely utilized in clinical diagnosis due to high safety, low-cost and portability.[6] As an US imaging contrast agents, gas precursor-contained microbubbles have developed to enhance contrast effect during the US imaging.[7, 8] However, gas precursor-contained US contrast agents have a limitation in passive-targeting of the tumor site after systemic administration due to their short half-life in blood stream and size barrier, which restricts extravasation from blood vessels to tumor tissues.[9, 10] In addition, the imaging resolution of US is relatively lower than other imaging approaches, and it can be interfered by bone, gas-filled organs. To overcome these limitations of US imaging, X-ray based CT can provide the merits, which deep tissue penetration, and rapid whole-body scanning with high resolution and 3D reconstruction.[11] Current x-ray CT imaging has practiced using low molecular iodinated contrast agents with high atomic number.[12] However, low molecular iodinated contrast agents could be rarely applicable in long-term and tumor-targeted imaging due to they have a short half-life in the body by the fast renal clearance.[13] In addition, high dosage of contrast agents is required to accurate x-ray CT imaging of tumor due to relative low sensitivity between tumor tissue and peripheral tissues. Thus, iodinated nanoparticles such as polymeric nanoparticles, micelles and liposomes, which could improve pharmacokinetics and tumor targeting effect, have

developed to solve limitations of low molecular iodinated contrast agents.[14-17]

Significant merits in both x-ray CT and US imaging can be complementary cooperated for development of multi-modal imaging agent, which can improve imaging sensitivity and provide definitive information of tumor. Dai and Tian et al., reported gold nanoshelled perfluorooctylbromide (PFOB) nanocapsules that could be utilized for dual-modal x-ray CT and US imaging *in vitro* and *in vivo* as well as photothermal ablation of tumors by photo-absorption effect.[18] In particular, they could obtain real-time imaging and additional anatomic information of tumor through x-ray CT and US dual-modal imaging by nanocapsules.

In this study, we proposed iodine containing diatrizoic acid (DTA)-conjugated glycol chitosan (GC) nanoparticles as a novel type of echogenic nanoparticles for the x-ray CT/US dual-modal imaging of tumor (Scheme 1). The DTA-conjugated GC nanoparticles (GC-DTA) were synthesized via amide bond formation between DTA and GC backbone (Figure 1a). In addition, 3,5-diacetamidobenzoic acid (DBA) conjugated GC nanoparticles (GC-DTA) were synthesized as a non-iodinated nanoparticles (Figure 1b). Then, bio-inert PFP-encapsulated GC-DTA nanoparticles (GC-DTA-PFP NPs) and GC-DBA nanoparticles (GC-DBA-PFP NPs) were prepared via oil in water (O/W) emulsion method (Figure 1c and Figure 1d). *In vitro* characteristics of the GC-DTA-PFP NPs, including hydrodynamic diameter, morphology, and cytotoxicity were investigated and x-ray CT/US dual-modal imaging efficacy of the GC-DTA-PFP NPs was evaluated. *In vivo* tumor accumulation of the GC-DTA-PFP NPs was monitored by the near-infrared fluorescence (NIRF) imaging. Finally, we observed *in vivo* x-ray CT/US dual-modal imaging efficacy in a SCC7 tumor-bearing mouse model. We expect that the GC-DTA-PFP NPs can be utilized for precise detection of the targeted tumor site by the x-ray CT imaging as well as real-time monitoring by the US imaging.
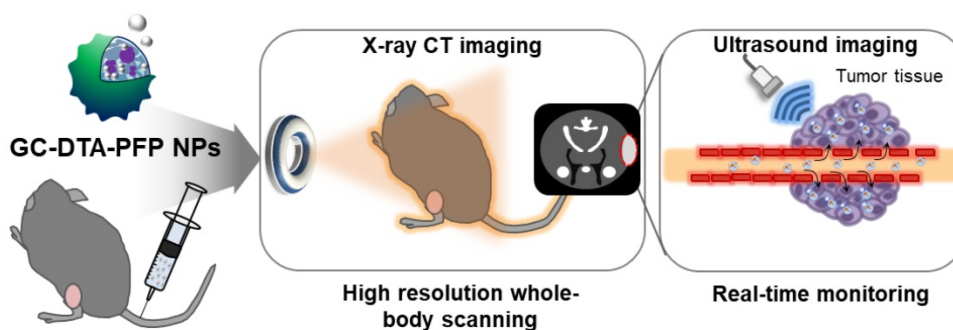
Scheme 1. Schematic illustration of x-ray CT/US dual-modal imaging using GC-DTA-PFP NPs. GC-DTA-PFP NPs can discrimination of tumor site by x-ray CT and real-time monitoring using US imaging.
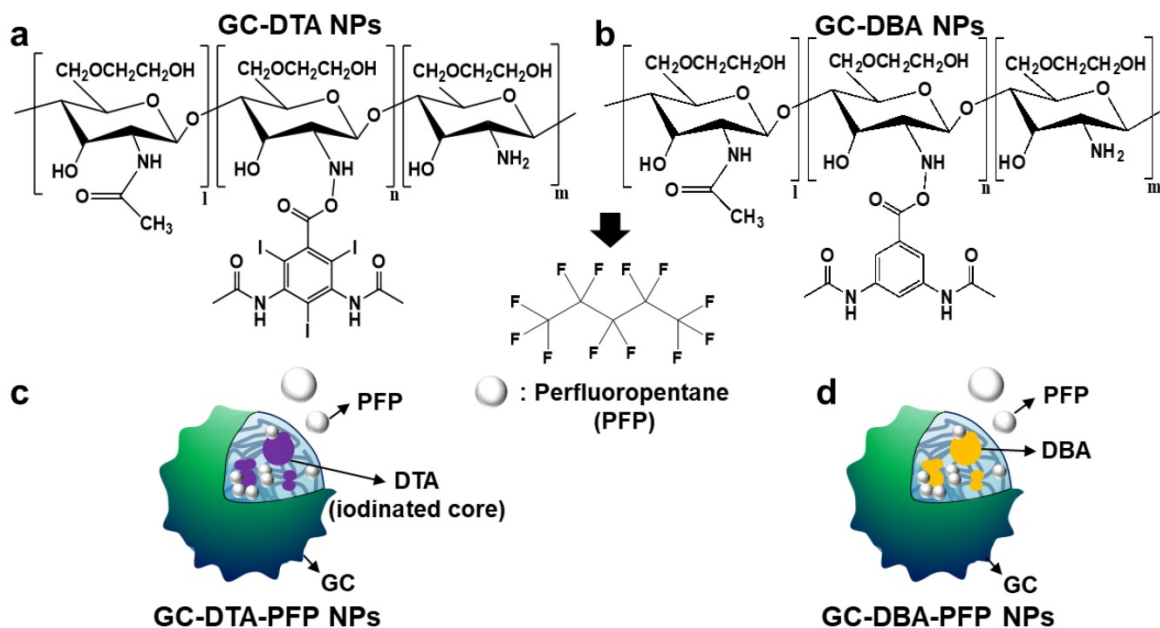
Figure 1. Synthetic scheme of (a) diatirizoic acid (DTA) and (b) 3,5-diacetamidobenzoic acid (DBA) conjugated glycol chitosan nanoparticles. (c) Schematic illustration of perfluoropentane (PFP) encapsulated DTA conjugated glycol chitosan nanoparticles (GC-DTA NPs) and DBA conjugated glycol chitosan nanoparticles (GC-DBA NPs) in aqueous conditions. (d) Schematic diagram of x-ray CT/US dual-modal imaging using GC-DTA-PFP NPs. GC-DTA-PFP NPs can discrimination of tumor site by x-ray CT and real-time monitoring using US imaging.

Results and Discussion

Preparation and characterization of GC-DTA-PFP and GC-DBA-PFP nanoparticles

To prepare x-ray CT/US dual-modal imaging agent, GC-DTA NPs, we used DTA as the iodine-contained radiocontrast agent in which utilized for x-ray CT imaging.[19-21] Diatrizoic acid (DTA)-conjugated self-assembled glycol chitosan (GC) nanoparticles (GC-DTA NPs) were prepared by chemical conjugation of GC and DTA via amide bond formation reaction. DTA was directly conjugated to the primary amine group of GC, which various molar ratios of 20 to 30 % in presence of EDC and NHS. In addition, we prepared 3,5-diacetamidobenzoic acid (DBA)-conjugated GC nanoparticles (GC-DBA NPs) as the non-iodinated nanoparticles. To confirm the chemical structures of GC-DTA NPs and GC-DBA NPs, they were freshly dissolved in DMSO-d_6 / D_2O (1:1 v/v) co-solvent and characteristic peaks were measured by 600 MHz ^{1}H-NMR (DD2 600 MHz FT NMR, Agilent Technologies, USA). The structures of GC-DTA NPs and GC-DBA NPs were analyzed using characteristic peaks at 2.4 - 2.6 ppm (-CH$_3$ at DTA and DBA) and 3.6 - 3.8 ppm (GC) and 7.6 - 7.9 ppm (-CH at DBA) (Figure 2a). The amount of iodine in GC-DTA NPs was determined using inductively coupled plasma mass spectrometry (ICP-MS). The amount of iodine in GC-DTA NPs was calculated 2.53 and 5.9 wt

% when the feed amount of DTA was 20% and 30%, respectively. For x-ray CT/US dual-modal imaging, 3 % (v/v) of perfluoropentane (PFP) was encapsulated into the GC-DTA NPs by oil in water (O/W) emulsion method.[22, 23] This is because that self-assembled GC-DTA NPs can provide the hydrophobic inner core due to the hydrophobic DTA molecules. In addition, the PFP which has strong hydrophobicity can interact with the multiple inner cores of the GC-DTA NPs, resulting in forming PFP-encapsulated GC-DTA NPs (GC-DTA-PFP NPs). As the non-iodinated nanoparticles, GC-DBA-PFP NPs were prepared through same method. Hydrodynamic diameter and size distribution of GC-DTA NPs and GC-DBA NPs were observed using dynamic laser scattering (DLS) after PFP encapsulation. Hydrodynamic diameters of GC-DTA NPs, GC-DBA NPs, GC-DTA-PFP NPs and GC-DBA-PFP NPs were 315 ± 49.52 nm, 303 ± 21.70 nm, 454.9 ± 3.33 nm and 498.5 ± 6.87 nm, respectively (Figure 2b). TEM images of GC-DTA NPs, GC-DBA NPs, GC-DTA-PFP NPs and GC-DBA-PFP NPs showed spherical morphology of particles (Figure 2c).

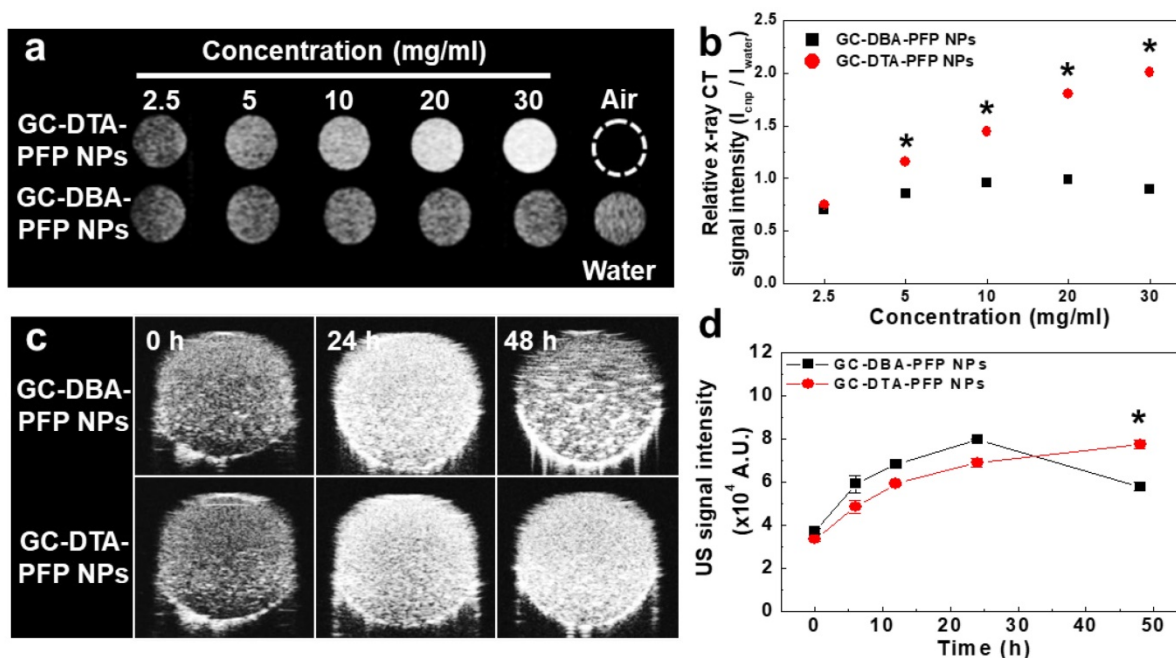### *In vitro* x-ray CT/US imaging of GC-DTA-PFP NPs and GC-DBA-PFP NPs

To observe x-ray absorption property of the GC-DTA-PFP NPs, x-ray CT images of GC-DTA-PFP NPs were acquired at the various concentrations (2.5 – 30 mg/ml of GC-DTA-PFP NPs). As shown in Figure 3a, x-ray absorption of the GC-DTA-PFP NPs

increased linearly according to the concentration of the GC-DTA-PFP NPs. However, x-ray absorption of the GC-DBA-PFP NPs showed negligible changes according to the concentration of the GC-DBA-PFP NPs. Figure 3b showed that relative x-ray CT signal intensities of the GC-DTA-PFP NPs and the GC-DBA-PFP NPs compared to the distilled water, respectively. X-ray absorption of GC-DTA-PFP NPs at 30 mg/ml showed 2.25-folds higher than that of GC-DBA-PFP NPs. This is implying that GC-DTA-PFP NPs were stable at high concentrations and x-ray was absorbed by iodine, effectively. Echogenicity of GC-DTA-PFP NPs and GC-DBA-PFP NPs was monitored using agar-gel phantom at the body temperature of 37 °C.[22, 23] As shown in Figure 3c and 3d, the echo signal of the GC-DTA-PFP NPs

gradually increased according to incubation time, and the signal persisted over 48 h. However, US signal of GC-DBA-PFP NPs was persisted 24 h and decreased at 48 h after incubation. This is because that GC-DTA NPs could provide the much stable inner core than GC-DBA NPs for encapsulation of PFP based on the halogen interaction between amine of GC back bone and iodine of DTA.[24] In addition, PFP-encapsulated self-assembled nanoparticles formulations could slowly and continuously arrive at the boiling point of PFP (> 29 °C), resulting in preventing the premature vaporization of PFP in physiological condition. Therefore, we expected that expansion of PFP in the GC-DTA-PFPs could be stably delayed in body temperature, and they could be utilized for further x-ray CT/US imaging *in vivo*.
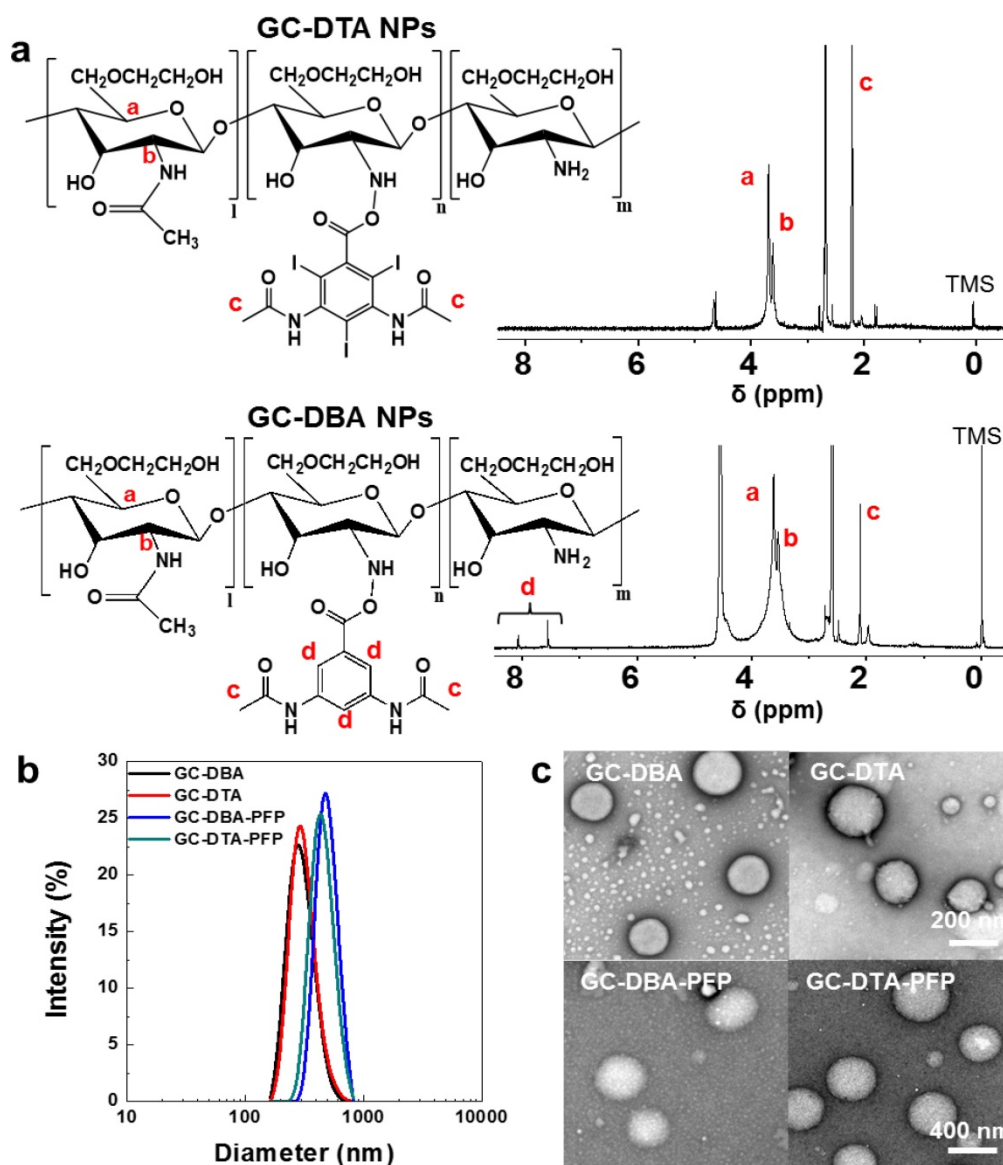
Figure 2. *In vitro* characterizations of GC-DTA NPs and GC-DBA NPs. (a) Structural analysis using ¹H-NMR. (b) Size distribution of GC-DTA NPs, GC-DBA NPs, GC-DTA-PFP NPs, and GC-DBA-PFP NPs by dynamic laser scattering (DLS) measurement. (c) TEM images of GC-DTA NPs, GC-DBA NPs, GC-DTA-PFP NPs, and GC-DBA-PFP NPs. Scale bar indicates 200 nm and 400 nm.

Figure 3. *In vitro* x-ray CT and US phantom images. (a) X-ray CT images of GC-DTA-PFP NPs and GC-DBA-PFP NPs (2.5 – 30 mg/ml). (b) Relative X-ray CT signal intensities of GC-DTA-PFP NPs and GC-DBA-PFP NPs. The error bars represent the standard deviation (n = 5). (c) Time-dependent US images of GC-DTA-PFP NPs and GC-DBA-PFP NPs at 37 ∘C. (d) Normalized US intensities of GC-DTA-PFP NPs and GC-DBA-PFP NPs. The error bars represent the standard deviation (n = 5). *Indicates difference at the *p* < 0.001 significance level.

In vitro cytotoxicity of analysis

The cytotoxicity of GC-DTA NPs, GC-DBA NPs, GC-DTA-PFP NPs and GC-DBA-PFP NPs was evaluated using both SCC7 cancer cells and NIH3T3 fibroblast cells. To determine the cytotoxicity of nanoparticles, SCC7 and NIH3T3 cells were incubated with GC-DTA NPs, GC-DBA NPs, GC-DTA-PFP NPs and GC-DBA-PFP NPs for 24 h and then cell viability was monitored by MTT assay. When SCC7 cells were treated with GC-DBA NPs and GC-DBA-PFP NPs, viabilities of SCC7 cells did not show significant changes, compared to the non-treated SCC7 cells (Figure 4a). However, GC-DTA NPs or GC-DTA-PFP NPs-treated SCC7 cells showed that their viabilities were decreased as the dose-dependent manner. This is because that DTA molecule has acute cellular toxicity such as cellular energy failure, disruption of calcium homeostasis, tubular cell polarity.[25, 26] Importantly, viability of GC-DTA NPs, GC-DBA NPs, GC-DTA-PFP NPs and GC-DBA-PFP NPs-treated NIH3T3 cells did not show significant changes, compared to the non-treated NIH3T3 cells (Figure 4b). Therefore, our results implying that GC-DTA-PFP NPs can be utilized as x-ray CT/US dual-modal imaging probe with biocompatibility.

### In vivo x-ray CT/US imaging of GC-DTA-PFP NPs and GC-DBA-PFP NPs

To evaluate the *in vivo* biodistibution of the GC-DTA-PFP NPs, 10 mg/kg of Cy5.5-labeled GC-DTA-PFP NPs (Cy5.5-GC-DTA-PFP NPs) were injected to SCC7 tumor bearing mice via I.V. injection and fluorescence signal in the body was monitored using the real-time near infrared fluorescence (NIRF) imaging system (eXplore Optix, ART Advanced Research Technologies Inc., Montreal, Canada). Cy5.5-GC-DTA-PFP NPs were began to accumulate into tumor tissue within 1 h post-injection and NIRF signal of tumor tissue was distinguished from the surrounding normal tissue, indicating the rapid tumor accumulation of Cy5.5-GC-DTA-PFP NPs. The NIRF intensity of Cy5.5-GC-DTA-PFP NPs maximally increased at 24 h post-injection, and it was clearly observed up to 48 h post-injection, indicating the long-retention time of Cy5.5-GC-DTA-PFP NPs at targeted tumor tissues (Figure 5a). Organ distribution and tumor accumulation of Cy5.5-GC-DTA-PFP NPs were precisely analyzed using the *ex vivo* NIRF signals from dissected tumors and organs, including liver, lung, spleen, kidney, and heart (Figure 5b). *Ex vivo* NIRF images after 48 h post-injection, strong NIRF intensities were mainly observed in tumor tissue and kidney. As shown in Figure 5c, the NIRF intensity of tumor tissues was 5 - 19.5 folds higher than those of liver, lung, spleen and heart, whereas the strong NIRF intensity was observed in the kidney. The filtration systems against foreign nanoparticles in the body are mainly related with liver and kidney. The kidney can

rapidly remove nanoparticles from the vascular with minimal catabolism or digestion in the body.[27] In addition, reticuloendothelial system (RES) in liver is a major excretion route with the renal clearance in kidney.[28] RES can recognize injected nanoparticles as foreign substance and eliminate most of them through phagocytosis. Therefore, unintended delivery of nanoparticles to liver is one of the major limitations in delivery using nanoparticles.[29] However, GC-DTA-PFP NPs showed high accumulation in both tumor tissue and kidney, not in liver. Therefore, this results significantly indicate that GC-DTA-PFP NPs can evade unintended excretion by RES in liver and prolong circulation *in vivo*.

Next, we obtained positively contrasted tumor x-ray CT images of SCC7 tumor bearing mice model using the GC-DTA-PFP NPs as an x-ray CT/US dual-modal imaging agent. To obtain positively contrasted tumor x-ray CT images, 120 mg/kg of GC-DTA-PFP NPs or GC-DBA-PFP NPs were directly injected (I.T.) into the SCC7 tumor tissues. As shown in Figure 6a, positively contrasted x-ray CT images of tumor tissues could obtain at 30 min post-injection, when they treated with 120 mg/kg of GC-DTA-PFP NPs. In contrast, x-ray CT signal of GC-DBA-PFP NPs showed negligible changes at 30 min post-injection. X-ray CT signal of GC-DTA-PFP NPs-treated tumor tissue was 1.6-folds higher than normal tissues. However, GC-DBA-PFP NPs-treated tumor tissue showed no significant signal changes between tumor tissue and normal tissue (Figure 6b). X-ray CT contrast effect of GC-DTA-PFP NPs and GC-DBA-PFP NPs was coincided with the *in vitro* x-ray CT phantom result. The *in vivo* tumor US images were obtained using US imaging system (Vevo770®) after I.V. injection of GC-DTA-PFP NPs (240 mg/kg, 0.3 mg/kg

of PFP) into SCC7 tumor-bearing mice. As shown in Figure 6c, the strong echo signals began to be observed at 1 h post-injection and gradually increased for 12 h, indicating that GC-DTA-PFP NPs could be accumulated in tumor tissue. And it was coincided with the NIRF biodistribution images of the GC-DTA-PFP NPs (Figure 5a). Moreover, echogenicity of GC-DTA-PFP NPs did feasible US imaging at deep tissue region of the SCC7 tumor. After 12 h and 24 h post-injection of the GC-DTA-PFP NPs, the echo signal in tumor tissue was 2.3- and 2.21-fold higher than pre-injection, respectively (Figure 6d). This is because that GC-DTA-PFP NPs could encapsulate PFP and retard evaporation of PFP, resulting in prolonging echogenicity in the physiological condition. In addition, the echogenicity of GC-DTA-PFP NPs in tumor tissue was coincided with NIRF accumulation property in Figure 5a. Therefore, we deduced from *in vivo* NIRF distribution and US imaging that GC-DTA-PFP NPs could deliver PFP to tumor tissue and persist echogenesis. Most of clinical US contrast agents have short signal half-life in the body, whereas persisted echo signals of GC-DTA-PFP NPs can be utilized for real-time US imaging to diagnosis of various diseases including tumor. For the evaluation of biosafety of GC-DTA-PFP NPs and GC-DBA-PFP NPs, major organs (liver, lung, spleen, kidney, and heart) were excised from GC-DTA-PFP NPs or GC-DBA-PFP NPs-treated mouse at 24 h after intravenous injection. Histopathological changes in the major organs were observed by hematoxylin and eosin (H&E) stain (Figure 7). GC-DAT-PFP NPs or GC-DBA-PFP NPs-treated mice did not show any pathological changes in the histology.
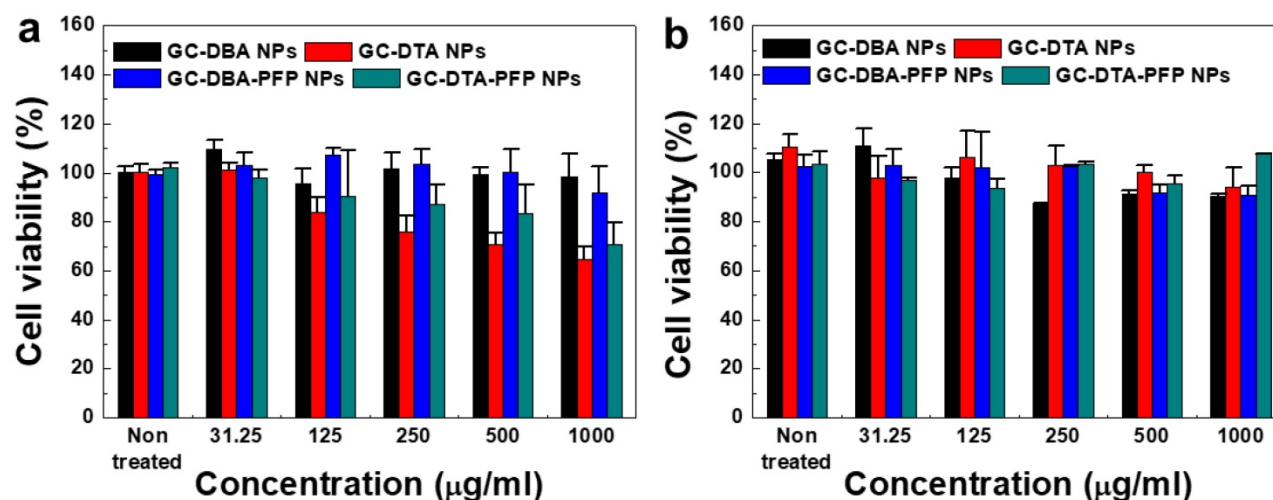
Figure 4. *In vitro* cytotoxicity of (a) SCC7 cells and (b) NIH3T3 cells which were incubated with GC-DTA NPs, GC-DBA NPs, GC-DTA-PFP NPs, or GC-DBA-PFP NPs for 24 h at 37 °C. The error bars represent the standard deviation (n = 5).
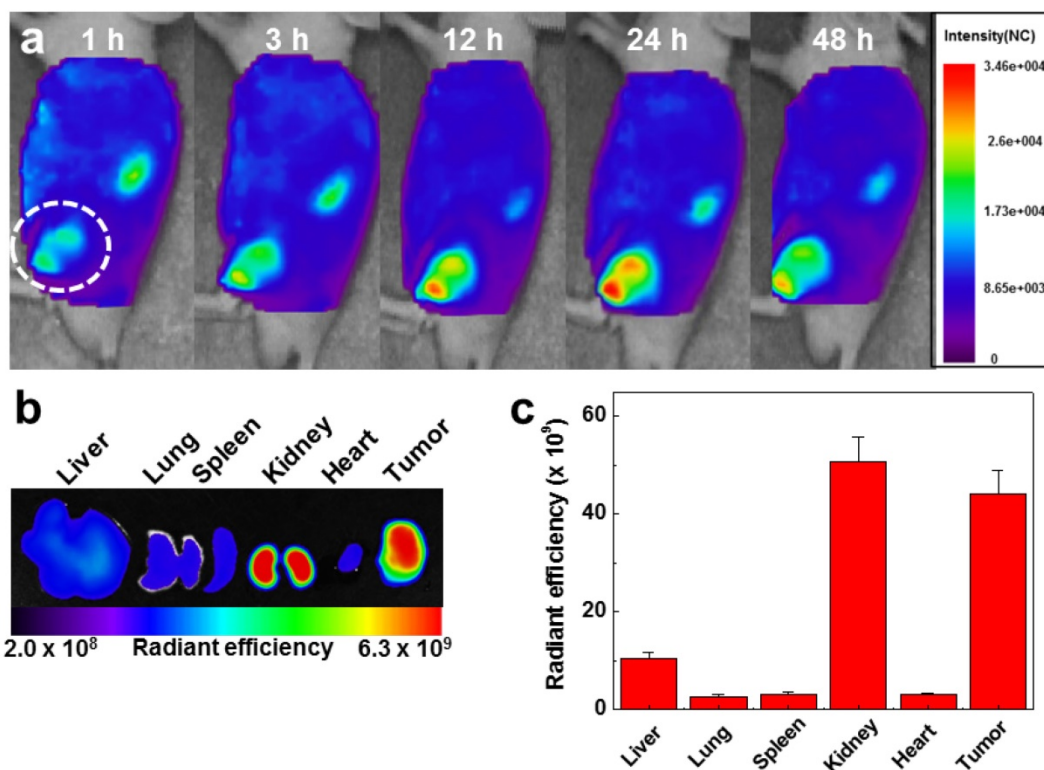
Figure 5. *In vivo* biodistribution of Cy5.5 labeled GC-DTA-PFP NPs in SCC7 tumor bearing mice (n = 3). (a) Whole-body near-infrared fluorescence (NIRF) images after intravenous injection of GC-DTA-PFP NPs (10 mg/kg). White circle indicates tumor site. (b) *Ex vivo* NIRF image of organs and tumor at 48 h post-injection of Cy5.5 labeled GC-DTA-PFP NPs. (c) NIRF intensities in the organs and tumor in (b). The error bar represents the standard deviation (n = 3).

In conclusion, we have demonstrated the feasibility of iodine containing-echogenic glycol chitosan nanoparticles (GC-DTA-PFP NPs) as an x-ray CT and US imaging agent of tumor diagnosis. PFP was successfully encapsulated into iodine containing inner core of GC-DTA NPs and formed stable nanoparticle in aqueous condition. GC-DTA-PFP NPs showed high stability and biocompatibility as well as enhancing both x-ray CT and US signal intensity *in vitro*. Moreover, GC-DTA-PFP NPs could enhance tumor x-ray CT imaging as well as US imaging *in vivo*. The outstanding properties of this dual-modal imaging agent could utilized for fast discrimination of tumor site by x-ray CT scanning and further real-time monitoring of the tumor site via US imaging. Therefore, we expected that iodinated echogenic nanoparticles-based x-ray CT/US dual-modal imaging may be applicable for diagnosis of various diseases including tumor. However, high dose of GC-DTA-PFP NPs which might have potential toxicity was required to improve x-ray absorption and US sensitivity *in vivo*. In addition, different dose and administration route of GC-DTA-PFP NPs for the dual-modal imaging can occur unintended side effects in the body. In further studies, we will optimize the potential toxicity and imaging sensitivity of iodinated echogenic nanoparticle, GC-DTA-PFP NPs, for the optimized x-ray CT/US dual-modal imaging probes.

Materials and methods

Materials

Glycol chitosan (GC, 250 kDa), diatrizoic acid (DTA), 3,5-diacetamidobenzoic acid (DBA), 1-ethyl-3-(3-dimethylaminopropyl)-carbodiimide hydrochloride (EDC), N-hydroxysuccinimide (NHS), dimethylsulfoxide (DMSO) and 3-(4,5-dimethylth-iazol-2-yl)-2,5-diphenyl tetrazolium bromide (MTT) were purchased from Sigma Aldrich (St. Louis, MO, USA). Perfluoropentane (PFP) 99% was purchased from Apollo Scientific Ltd. (Manchester, UK). All the chemicals were analytical grade and used without further purification. Squamous cell carcinoma (SCC7) and mouse embryonic fibroblast cell (NIH3T3) were purchased from American Type Culture Collection (Rochkvile, MD, USA). RPMI 1640 media, fetal bovine serum (FBS), antibiotics (streptomycin and 100 U/mL penicillin) and Dulbecco's phosphate buffered saline (DPBS, pH 7.4) were purchased from WelGENE Inc. (Daegu, Republic of Korea).
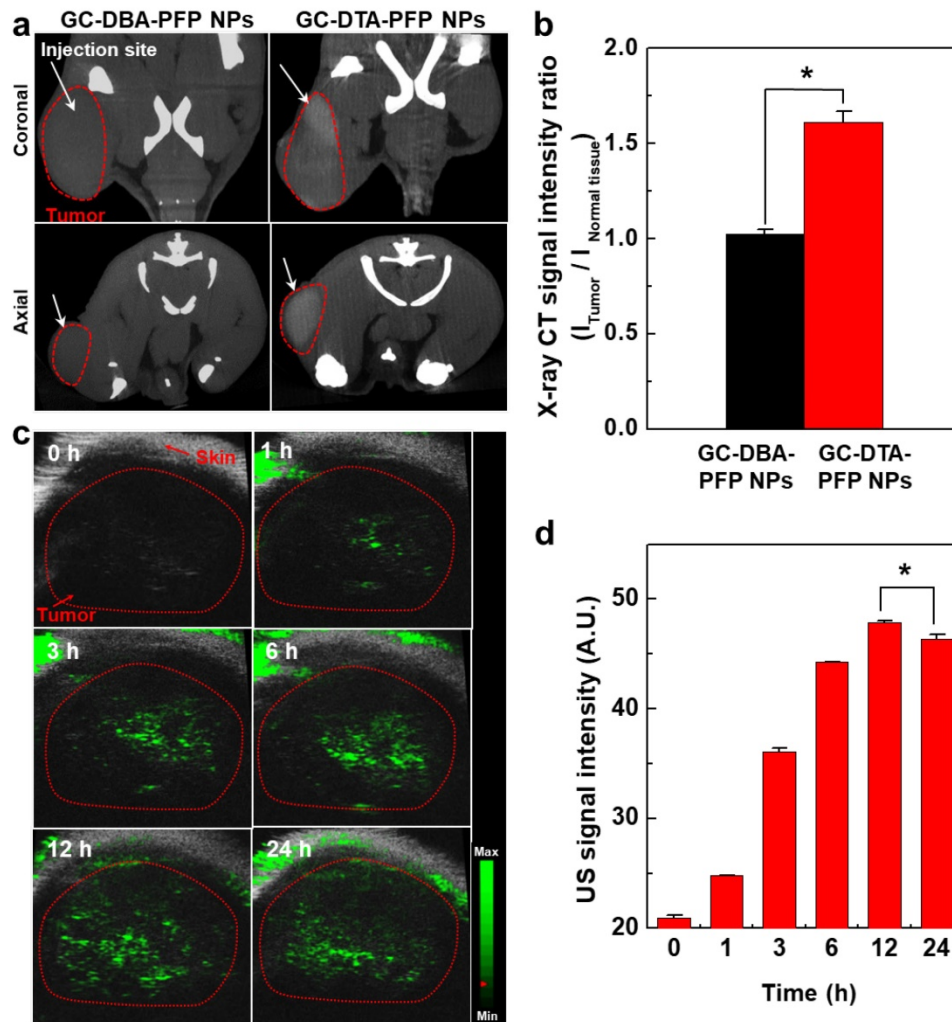
Figure 6. *In vivo* x-ray CT/US imaging in SCC7 tumor-bearing mice (n = 3). (a) X-ray CT images of 120 mg/kg of GC-DTA-PFP NPs (7 mg/kg of iodine) and GC-DBA-PFP NPs-treated SCC7 tumor-bearing mice, respectively. The white arrows indicate the direct-injection site in tumor tissue. (b) Relative x-ray CT signal intensities of GC-DTA-PFP NPs and GC-DBA-PFP NPs. The relative x-ray CT signal intensities were calculated by intensities ratio of normal tissues to tumor tissue. The error bars represent the standard deviation (n = 3). (c) Time-dependent US images of tumor tissue after intravenous injection of GC-DTA-PFP NPs (240 mg/kg, 0.3 mg/kg of PFP) into SCC7 tumor-bearing mice (n =3). (d) Time-dependent US signal intensities at tumor site. The error bars represent the standard deviation (n = 3). *Indicates difference at the *p* < 0.005 significance level.
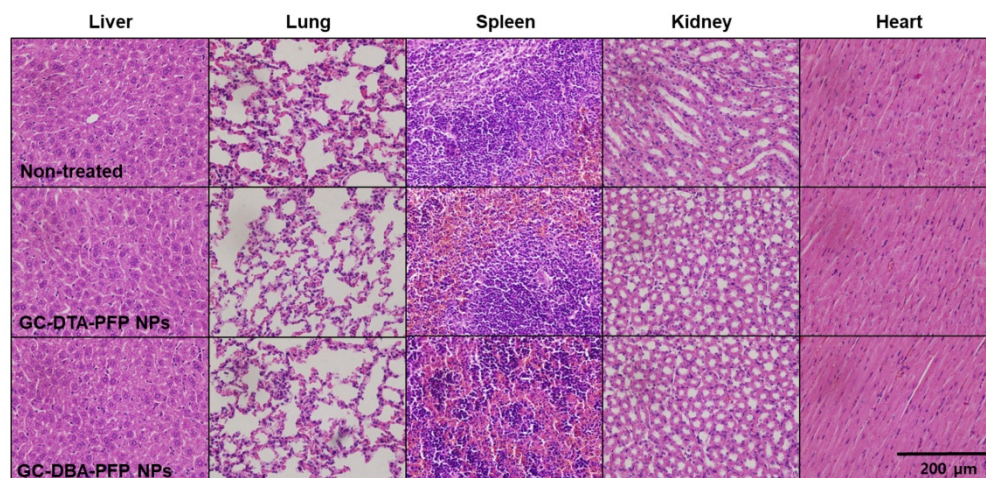
Figure 7. Biosafety of GC-DTA-PFP NPs and GC-DBA-PFP NPs was evaluated by histopathological changes in the major organs (liver, lung, spleen, kidney, heart) based on H&E staining.

Synthesis of diatrizoic acid conjugated glycol chitosan nanoparticle (GC-DTA NPs) and 3,5-diacetamidobenzoic acid (DBA) conjugated glycol chitosan nanoparticles (GC-DBA NPs)

Iodinated glycol chitosan nanoparticles (GC-DTA) were synthesized by chemical conjugation of diatrizoic acid (DTA) to glycol chitosan (GC) backbone. In brief, 750 mg of GC was dissolved in 750 ml of deionized water (DIW). The solution was stirred for 24 h at room temperature under reflux condition. After that, DTA (523.5 mg) was dissolved in 5 ml of DMSO and then 5 ml of DIW was added into the DTA solution. EDC (249 mg) and NHS (148.5 mg) were dissolved in each 2 ml of DIW. EDC and NHS solutions are mixed with DTA solution and stirring for 30 min. The solution was dropwised into the GC solution. The mixed solution was vigorously stirred for 12 h at room temperature. And then purified by dialysis against DIW for 3 days using dialysis membrane (MWCO: 12-14 kDa, Spectra-Por, USA). The resulting solution was lyophilized to obtain white powder, GC-DTA NPs. As a control nanoparticle, 3,5-diacetamidobenzoic acid (DBA) conjugated GC nanoparticles (GC-DBA NPs) were synthesized by described above. In brief, 750 mg of GC was dissolved in 750 ml of deionized water (DIW). The solution was stirred for 24 h at room temperature under reflux condition. After that, DBA (130 mg) was dissolved in 5 ml of DMSO and 5 ml of DIW was added to DBA solution. EDC (61.8 mg) and NHS (36.8 mg) were dissolved in each 2 ml of DIW. EDC and NHS solutions are mixed with DTA solution and stirring for 30 min. The solution was dropwised into the GC solution. The mixed solution was vigorously stirred for 12 h at room temperature and then purified by dialysis against DIW for 3 days using dialysis membrane (MWCO: 12-14 kDa, Spectra-Por, USA). The resulting solution was lyophilized to obtain white powder, GC-DBA NPs. For *in vivo* near infrared fluorescence (NIRF) imaging, Cy-5.5 labeled GC-DTA NPs were prepared by following process. 30 mg of GC-DTA NPs were dissolved in 15 ml of DMSO/DIW (50:50 v/v). Cy5.5-NHS (0.5 mg) was dissolved in DMSO and dropwised into GC-DTA NPs solution. The mixed solution was vigorously stirred for 12 h at room temperature and then purified by dialysis against DIW for 3 days using dialysis membrane (MWCO: 12-14 kDa, Spectra-Por, USA). The resulting solution was lyophilized to obtain sky blue powder, Cy5.5-GC-DTA NPs.

Preparation of perfluoropentane encapsulated GC-DTA NPs (GC-DTA-PFP NPs) and GC-DBA NPs (GC-DBA-PFP NPs)

Perfluoropentan encapsulated GC-DTA NPs (GC-DTA-PFP NPs) and GC-DBA NPs (GC-DBA-PFP NPs) were formulated by o/w emulsification method as described in previous reports.[22, 23] In brief, 30 mg of GC-DTA NPs were dissolved in 1 ml of DIW and solution was contained into ice bath and emulsified with a probe type sonicator (Ultrasonic processor 750-Watt, Cole-Parmer, IL, USA). 30 µl of PFP (3% v/v, oil phase) was slowly dropped into the GC-DTA NPs solution, with sonication process (23% power, 30 sec on, 5 sec off) during 1 min. GC-DBA-PFP NPs were also prepared as described above.

Characterization of GC-DTA NPs, GC-DBA-NPs, GC-DTA-PFP NPs and GC-DBA-PFP NPs

To confirm of chemical structures of GC-DTA NPs and GC-DBA NPs, they were freshly dissolved in DMSO-d_6 / D_2O (1:1 v/v) and characteristic peaks were measured by 600 MHz ^{1}H-NMR (DD2 600 MHz FT NMR, Agilent Technologies, USA). The structure of GC-DTA NPs and GC-DBA NPs were analyzed using characteristic peaks at 2.4-2.6 ppm (-CH3 at DTA and DBA) and 3.6-3.8 ppm (GC) and 7.6-7.9 ppm (-CH at DBA) (Figure 2a). The amount of iodine in GC-DTA NPs were determined using the inductively coupled plasma optical emission spectroscopy (ICP-AES, 710-ES, Varian, Australia). To analyze the size distribution and zeta-potential (ξ) of GC-DTA NPs, GC-DBA-NPs, GC-DTA-PFP NPs and GC-DBA-PFP NPs, 1 mg of GC-DTA NPs, GC-DBA-NPs, GC-DTA-PFP NPs and GC-DBA-PFP NPs were dispersed in 1 ml of phosphate buffered saline (PBS, pH 7.4) and were measured size with zeta-potential using Zeta-sizer (Nano ZS, Malvern, UK) (Figure 2b). The morphologies of GC-DTA NPs, GC-DBA-NPs, GC-DTA-PFP NPs and GC-DBA-PFP NPs were observed using transmission electron microscope (TEM, Tecnai F20, FEI, Netherlands) at an accelerating voltage of 200 keV (Figure 2c). For TEM images, all samples were dispersed in distilled water and were negative stained by 2 % uranyl acetate.

In vitro x-ray CT and US phantom imaging of GC-DTA-PFP NPs and GC-DBA-PFP NPs

To determine the x-ray absorption of GC-DTA-PFP NPs and GC-DBA-PFP NPs, they were freshly dispersed in the DIW. And then, GC-DTA-PFP NPs and GC-DBA-PFP NPs were diluted with DIW according various concentration (2.5 mg/ml to 30 mg/ml). X-ray absorption was measured using

micro-computed tomography (Skyscan 1076, Skyscan Inc., Belgium) (Figure 3a). For x-ray CT images were obtained by the following protocol: 65 kVp, 60 µA, 26.7 × 26.7 mm field of view, 0.053 × 0.053 × 0.054 mm^3 voxel size, 500 ms per frame, 360 views, 512 × 512 reconstruction matrix, and 400 slices. The relative x-ray CT signal intensity was calculated using Image J software (National Institutes of Health, Bethesda, USA) (Figure 3b). *In vitro* US phantom images of GC-DTA-PFP NPs and GC-DBA-PFP NPs were obtained using High-Resolution Micro-Imaging System (Vevo 770 system, Visual Sonics, Toronto, Canada) and equipped with RMV 706 US probe, as described in previous reports.[22, 23] For *in vitro* US phantom imaging, 200 µl of GC-DTA-PFP NPs and GC-DBA-PFP NPs solutions were injected into the agar-phantom molds and 40 MHz of ultrasound signal was applied at samples for proper US imaging (Figure 3c). US signal intensity was calculated by subtracted ROI ratios between water control and sample's intensity (Figure 3d).

In vitro cell cytotoxicity assays

SCC7 cells were cultured in RPMI 1640 medium containing 10% (v/v) FBS and 1% (v/v) penicillin–streptomycin at 37 ◦C in a humidified 5% CO_2 incubator. NIH3T3 cells were cultured in DMEM (Dulbecco Modified Eagle Medium) containing 10% (v/v) FBS and 1% (v/v) penicillin–streptomycin at 37 ◦C in a humidified 5% CO_2 incubator. The cytotoxicity of GC-DTA NPs, GC-DBA-NPs, GC-DTA-PFP NPs and GC-DBA-PFP NPs was evaluated using the MTT assay (Figure 4). In brief, 5 × 10^3 cells of SCC7 and NIH3T3 cells were seeded onto 96-well plate and stabilized for 24 h. After stabilizing, the cells were washed twice with DPBS and incubated for 24 h with various concentrations of GC-DTA NPs, GC-DBA-NPs, GC-DTA-PFP NPs and GC-DBA-PFP NPs. Then, 25 µL of the MTT solution (0.5 mg/mL in the medium) was added to each well. And then the cells were incubated for an additional 40 min at 37 ºC. MTT-containing media was removed and then SCC7 and NIH3T3 cells were dissolved in 200 µL of DMSO. The absorbance of each well was measured at 570 nm using a microplate reader (VERSAmaxTM, Molecular Devices Corp., Sunnyvale, CA).

In vivo and *ex vivo* distribution analysis by near-infrared fluorescence (NIRF) imaging

All experiments with live animals were performed in compliance with the relevant laws and institutional guidelines of Korea Institute of Science and Technology (KIST) and institutional committees have approved the experiments. For the NIRF imaging of Cy5.5-GC-DTA-PFP NPs, athymic nude mice (5-weeks old, 18 - 20 g, male) were purchased from Orient Bio Inc. (Gyeonggi-do, Korea). Fur of the mouse could interfere with fluorescence imaging through absorbing and scattering light during the image acquisition. In this point of view, the nude mouse is an optimized for near-infrared fluorescence imaging. Therefore, SCC7 tumor-bearing nude mouse were utilized for clear observation of *in vivo* and *ex vivo* distribution of GC-DTA-PFP NPs. To prepare tumor-bearing mice models, a suspension of 1x 10^6 SCC7 cells in RPMI1640 (80 µl) was subcutaneously injected into left flanks of mice. When tumors grew to approximately 350 – 500 mm^3 in volume, 10 mg/kg of Cy5.5-GC-DTA-PFP NPs was injected into the mice via tail vein (n = 3). The time-dependent biodistribution and accumulation profiles of Cy5.5-GC-DTA-PFP NPs were observed by using an eXplore Optix system with 670 nm-pulsed laser diode (Advanced Research Technologies Inc., Montreal, Canada) (Figure 5a). To observe NIRF in major organs, each mice was sacrificed 48 h post-injection. Then, major organs with tumors were excised and NIRF image was measured using the IVIS Lumina Series III (PerkinElmer, Massachusetts, USA) (Figure 5b). Fluorescence intensities in organs were analyzed using the Living Image® software (PerkinElmer, Massachusetts, USA) (Figure 5c).

X-ray CT/US imaging of GC-DTA-PFP NPs and GC-DBA-PFP NPs in tumor-bearing mice

For the x-ray CT/US dual-modal imaging of GC-DTA-PFP NPs and GC-DBA-PFP NPs, C3H/HeN mice (5-weeks old, 18 - 20 g, male) were purchased from Orient Bio Inc. (Gyeonggi-do, Korea). To prepare tumor-bearing mice models, a suspension of 1x 10^6 SCC7 cells in RPMI1640 (80 µl) was subcutaneously injected into left flanks of mice. To feasible *in vivo* x-ray CT imaging of GC-DTA-PFP NPs and GC-DBA-PFP NPs, 120 mg/kg of GC-DTA-PFP NPs (7 mg/kg of iodine) and GC-DBA-PFP NPs were directly injected into tumor tissues (n = 3) when the SCC7 tumors grew to approximately 350 – 500 mm^3 in volume. For x-ray CT images were obtained by the following protocol: 65 kVp, 60 µA, 26.7 × 26.7 mm field of view, 0.053 × 0.053 × 0.054 mm^3 voxel size, 500 ms per frame, 360 views, 512 × 512 reconstruction matrix, and 600 slices (Figure 6a). The relative x-ray CT signal intensity was calculated using Image J software (National Institutes of Health, Bethesda, USA) (Figure 6b). For *in vivo* US imaging, 240 mg/kg (0.3 mg/kg of PFP) of GC-DTA-PFP NPs and GC-DBA-PFP NPs were intravenously injected to SCC7 tumor-bearing mouse (n = 3). Then, US images of tumor tissues were observed for 24 h using High-Resolution Micro-Imaging System (Vevo 770

system, Visual Sonics, Toronto, Canada) equipped with RMV 706 US probe and 40 MHz of ultrasound signal (Figure 6c). US signal intensity was calculated by subtracted ROI ratios between background and sample's intensity (Figure 6d).

Histological analysis

For evaluation of biosafety of GC-DTA-PFP NPs and GC-DBA-PFP NPs, major organs (liver, lung, spleen, kidney, and heart) were excised from GC-DTA-PFP NPs or GC-DBA-PFP NPs-treated mouse at 24 h after intravenous injection, and they were fixed with 4 % paraformaldehyde solution and embedded in paraffin. The sliced organs (5 μm) were stained by Hematoxylin and Eosin (H&E) and observed by optical microscope (BX 51, Olympus, USA).

Statistical analysis

In this study, the differences between experimental and control groups were analyzed using one-way ANOVA and considered statistically significant (marked with an asterisk (*) in figure) if $p < 0.05$.

Acknowledgements

Competing Interests

The authors have declared that no competing interest exists.

References

1. Key J, Leary JF. Nanoparticles for multimodal in vivo imaging in nanomedicine. International journal of nanomedicine. 2014; 9: 711.
2. Kim J, Piao Y, Hyeon T. Multifunctional nanostructured materials for multimodal imaging, and simultaneous imaging and therapy. Chemical Society Reviews. 2009; 38: 372-90.
3. Pysz MA, Gambhir SS, Willmann JK. Molecular imaging: current status and emerging strategies. Clinical Radiology. 2010;65: 500-16.
4. Willmann JK, van Bruggen N, Dinkelborg LM, Gambhir SS. Molecular imaging in drug development. Nat Rev Drug Discov. 2008; 7: 591-607.
5. Zhang K, Chen H, Li P, Bo X, Li X, Zeng Z, et al. Marriage Strategy of Structure and Composition Designs for Intensifying Ultrasound & MR & CT Trimodal Contrast Imaging. ACS Appl Mater Interfaces. 2015; 7: 18590-9.
6. Li X, Zhang XN, Li XD, Chang J. Multimodality imaging in nanomedicine and nanotheranostics. Cancer Biol Med. 2016; 13: 339-48.
7. Stewart VR, Sidhu PS. New directions in ultrasound: microbubble contrast. Br J Radiol. 2006; 79: 188-94.
8. Hizoh I, Strater J, Schick CS, Kubler W, Haller C. Radiocontrast-induced DNA fragmentation of renal tubular cells in vitro: role of hypertonicity. Nephrol Dial Transplant. 1998; 13: 911-8.
9. Yin T, Wang P, Zheng R, Zheng B, Cheng D, Zhang X, et al. Nanobubbles for enhanced ultrasound imaging of tumors. International Journal of Nanomedicine. 2012; 7: 895-904.
10. Son S, Min HS, You DG, Kim BS, Kwon IC. Echogenic nanoparticles for ultrasound technologies: Evolution from diagnostic imaging modality to multimodal theranostic agent. Nano Today. 2014; 9: 525-40.
11. Lee N, Choi SH, Hyeon T. Nano-sized CT contrast agents. Adv Mater. 2013; 25: 2641-60.
12. Yu SB, Watson AD. Metal-Based X-ray Contrast Media. Chem Rev. 1999; 99: 2353-78.
13. Singh J, Daftary A. Iodinated contrast media and their adverse reactions. J Nucl Med Technol. 2008; 36: 69-74; quiz 6-7.
14. Elrod DB, Partha R, Danila D, Casscells SW, Conyers JL. An iodinated liposomal computed tomographic contrast agent prepared from a diiodophosphatidylcholine lipid. Nanomedicine. 2009; 5: 42-5.
15. de Vries A, Custers E, Lub J, van den Bosch S, Nicolay K, Grull H. Block-copolymer-stabilized iodinated emulsions for use as CT contrast agents. Biomaterials. 2010; 31: 6537-44.
16. Anton N, Vandamme TF. Nanotechnology for computed tomography: a real potential recently disclosed. Pharmaceutical research. 2014; 31: 20-34.
17. Lim C-K, Shin J, Kwon IC, Jeong SY, Kim S. Iodinated Photosensitizing Chitosan: Self-Assembly into Tumor-Homing Nanoparticles with Enhanced Singlet Oxygen Generation. Bioconjugate Chemistry. 2012; 23: 1022-8.
18. Ke H, Yue X, Wang J, Xing S, Zhang Q, Dai Z, et al. Gold nanoshelled liquid perfluorocarbon nanocapsules for combined dual modal ultrasound/CT imaging and photothermal therapy of cancer. Small (Weinheim an der Bergstrasse, Germany). 2014; 10: 1220-7.
19. Peng C, Li K, Cao X, Xiao T, Hou W, Zheng L, et al. Facile formation of dendrimer-stabilized gold nanoparticles modified with diatrizoic acid for enhanced computed tomography imaging applications. Nanoscale. 2012; 4: 6768-78.
20. Liu H, Xu Y, Wen S, Zhu J, Zheng L, Shen M, et al. Facile hydrothermal synthesis of low generation dendrimer-stabilized gold nanoparticles for in vivo computed tomography imaging applications. Polymer Chemistry. 2013; 4: 1788-95.
21. Guo R, Wang H, Peng C, Shen M, Zheng L, Zhang G, et al. Enhanced X-ray attenuation property of dendrimer-entrapped gold nanoparticles complexed with diatrizoic acid. Journal of Materials Chemistry. 2011; 21: 5120-7.
22. Min HS, Son S, Lee TW, Koo H, Yoon HY, Na JH, et al. Liver-Specific and Echogenic Hyaluronic Acid Nanoparticles Facilitating Liver Cancer Discrimination. Adv Funct Mater. 2013; 23: 5518-29.
23. Min HS, You DG, Son S, Jeon S, Park JH, Lee S, et al. Echogenic Glycol Chitosan Nanoparticles for Ultrasound-Triggered Cancer Theranostics. Theranostics. 2015; 5: 1402-18.
24. Yada H, Tanaka J, Nagakura S. Charge-transfer complexes between iodine and various aliphatic amines. Bulletin of the Chemical Society of Japan. 1960; 33: 1660-7.
25. Haller C, Hizoh I. The Cytotoxicity of Iodinated Radiocontrast Agents on Renal Cells In Vitro. Investigative Radiology. 2004; 39: 149-54.
26. Hasebroock KM, Serkova NJ. Toxicity of MRI and CT contrast agents. Expert Opinion on Drug Metabolism & Toxicology. 2009; 5: 403-16.
27. Kean T, Thanou M. Biodegradation, biodistribution and toxicity of chitosan. Advanced Drug Delivery Reviews. 2010; 62: 3-11.
28. Longmire M, Choyke PL, Kobayashi H. Clearance Properties of Nano-sized Particles and Molecules as Imaging Agents: Considerations and Caveats. Nanomedicine (London, England). 2008; 3: 703-17.
29. Li SD, Huang L. Nanoparticles evading the reticuloendothelial system: role of the supported bilayer. Biochim Biophys Acta. 2009; 1788: 2259-66.